Data Repository Item

Preparation

One valve of each specimen was coated with J-B® KWIK Weld™ epoxy resin, mounted on a plexiglas cube using Devcon® High Strength Plastic Welder™, and cut along the axis of maximum growth with a Wirtz-Buehler® low speed saw. In order to clarify inter-annual growth patterns, the sections were ground on glass plates (800 and 1200 grit powder) and polished on a lap (1 μm). The samples were etched in a solution of 0.5% acetic acid, 12.5% glutaraldehyde and 5g alcian blue powder at 37 to 40°C for 25 min, carefully rinsed in de-ionized water (Mutvei et al., 1996), dehydrated in a series of graded EtOH, bathed in hexamethydisilazane (99%) for 30min, and allowed to air-dry (Schöne and Bentley, 2002). Etching increased the contrast of the growth increments, Glutaraldehyde, EtOH and HMDS were used to preserve the organic matrix of the shells.

Measurements

For precise determination of growth rates, annual increments (see Figure DR1) were viewed under a reflective light binocular microscope (magnification up to 400 X), digitized with a Nikon Coolpix® 995 camera and measured to the nearest 1μm with Scion/NIH version 4.0.2 beta image analysis software (available free at http://www.scioncorp.com). We measured the increment widths in the outer shell layer parallel to the outer shell surface.

Detrending and Standardization

The growth of most organisms is controlled by physiological constraints and environmental conditions. Analysis of environmental signals in growth increment time-series requires removal of ontogenetic growth trends, predominantly age-related growth trends. As the shell grows older, the rate and the year-to-year variance decrease. Statistical methods for detrending were developed by dendrochronologists (for a review see Cook and Kairiukstis, 1990). In the present study we used logistic growth functions and polynomials to estimate the growth curves. We then calculated growth indices (GI) by dividing measured by predicted (estimated) growth values at each year. Finally, the GI data were standardized by subtracting the mean of the GI time series and dividing by the standard deviation of the GI time series. Methods are described in more detail in a variety of publications (Cook and Kairiukstits, 1990, Schöne, 2003).

Individual SGI chronologies

Individual SGI time series (see Figure DR2) over the period 1757-1861 and 1866-2001 show a high degree of running similarity (73.2%, $p<0.05$). Accordingly, the 95% confidence bands of the mean curves (see Figure DR3) are narrow. The number of specimens used per year is given in see Figure DR4.

Wavelet analysis

Real-world signals are usually limited in time and frequency. Proper analysis of such signals require a compromise between functions used for the analysis of time-limited signals (e.g. block functions) and functions used for the analysis of band-limited signals (e.g. Fourier transforms). Such analysis is possible through the application of wavelets (small waves; ondelette).
Wavelet decomposition can detect local features of a signal and allows for multi-level resolution (scale) of a signal. Results are displayed as a variance map revealing phases of coherency and incoherency a function of time. While a Fourier transform gives only an estimation of the overall frequencies contained in a signal, the wavelet transform resolves the localized frequency and intensity patterns of a signal. Wavelet transforms can resolve if and how a signal's strength changed over time; it can analyze intermittently stronger or weaker periods of the signal.
The wavelet coefficient $W_f(a,\tau)$ of a function $f(t)$ is produced through the convolution of f and a dilated function ψ (the so-called wavelet mother or parent wavelet):

$$W_f(a,\tau) = \frac{1}{\sqrt{a}} \int_{-\infty}^{\infty} f(t)\psi\left(\frac{t-\tau}{a}\right)dt,$$

where a is the dilation parameter denoting the local scale center (comparable to the frequency in the Fourier analysis), t is time, and τ representing the local time center. In the present study we used the Morlet wavelet, a Gaussian-windowed complex sinusoid,

$$\psi(t) = e^{i\omega_0 t} e^{-t^2/2},$$

because it offers the best frequency localization. For an excellent mathematical presentation of wavelet analyses the reader is referred to Daubechies (1988) and for subtleties of applying wavelet transforms to real-world data see Torrence and Compo (1998).

Wavelet transforms of unfiltered *A. islandica*-based and Hurrell's instrumental WNAO indices are depicted in Figure DR5.

Cross-correlation wavelet analysis

Cross-correlation wavelet analysis (e.g., Torrence and Webster, 1999, Gurley et al., 2003) helps to understand where the phases of two signals are coherent and at which strength. Comparison of two continuous wavelet transforms $W_f(a,\tau)$ and $W_g(a, \tau)$ of the chronologies $f(t)$ and $g(t)$ can be performed in many ways, e.g. through a visual approach (as done in the present paper) or mathematically.

Visual comparison of various wavelet spectra has several advantages over cross-correlation wavelet analysis (see Fig. DR6). (1) Fewer diagrams (here: six) are needed to show similar patterns among different spectra. Cross-spectral analysis compares only two time-series at a time. For example, fifteen spectra were required in the present case. (2) Existing cross-spectral wavelet analysis techniques only focus on coherency between two wavelet spectra. Individual wavelet transforms are multiplied, so that signals present at the same time interval and the same frequency in both spectra are amplified. Such methods are

not suitable to show whether weak signals occur in both wavelet transforms or only in one. For example, the following information does not show up in the cross-correlation spectra. Visual comparison (Text Fig.3) reveals that the coherent interval in our *A. islandica*–based WNAO proxy chronology during the second part of the 20th century occurs about ten years later than in instrumental and other proxy WNAO time-series. In Cook's et al. (2002) WNAO index this coherent interval ends about eight years earlier than in other proxy and instrumental WNAO records. The coherent interval during the period of 1935-1947 appears very strong in our new proxy and Glueck and Stockton's (2001) WNAO index, but weak in other chronologies. Sharp signals occur during the period of 1908-1923 in Jones' et al. (1997) instrumental WNAO and the *A. islandica*–based WNAO, whereas other instrumental and proxy WNAO chronologies show only weak (Hurrell, 1995; Luterbacher et al., 2001; Glueck and Stockton, 2001) or no coherency (Cook et al., 2002) during that time.

Cross-spectral wavelet analysis is described in the following. The wavelet cross-scalogram can be calculated as the product of the wavelet transforms $W_f(a,\tau)$ and $W_g(a,\tau)$: $W_{fg}(a,\tau) = W_f(a,\tau)^* W_g(a,\tau)$, where $W_f(a,\tau)^*$ is the complex conjugate of $W_f(a,\tau)$. (According to the Correlation Theorem it is also possible to first determining the correlation between the functions $f(t)$ and $g(t)$ and then performing a spectral analysis of the combined function.) The wavelet cross-scalograms of our new proxy WNAO and instrumental/other proxy WNAO indices are given in see Figure DR6. Intensity maxima indicate where the two time-series share coherent phases (e.g. during the periods of c. 1830–1855 and after c. 1978).

Running correlation

We calculated running correlation coefficients within a sliding 30-yr window between our *A.islandica*-based WNAO index with instrumental and other proxy WNAO chronologies. The result is shown in see Figure DR7. During recent times the correlation between our new proxy and other WNAO indices is highest (up to $r = 0.80$). Toward the mid 18th century the correlation decreases. We attribute this finding to the decreasing quality of proxy records in older periods. Our WNAO proxy record, for example, consists of only two specimens prior to 1861.

References

Cook, E.R., and Kairiukstis, L.A., eds., Methods of Dendrochronology, 1990, Applications in the Environmental Sciences: Dordrecht, Kluver, 394 p.

Cook, E.R., D'Arrigo, R.D., and Mann, M.E., 2002, A well-verified, multiproxy reconstruction of the winter North Atlantic Oscillation Index since A.D. 1400: Journal of Climate, v. 15, p. 1754–1764.

Daubechies, I., Orthonormal basis of compactly supported wavelets: Comm. Pure and applied maths, v. 41, p. 909-996.

Glueck, M.F., and Stockton, C.W., 2001, Reconstruction of the North Atlantic Oscillation: International Journal of Climatology, v. 21, p. 1453–1465.

Gurley, K., Kijewski, T., and Kareem, A., 2003, First- and higher-order correlation detection using wavelet transforms: Journal of Engineering Mechanics, v. 129, p. 188-201.

Hurrell, J.W., 1995, Decadal trends in the North Atlantic oscillation: Regional temperatures and precipitation: Science, v. 269, p. 676–679.

Jones, P.D., Jónsson, T., and Wheeler, D., 1997, Extension to the North Atlantic Oscillation using early instrumental pressure observations from Gibraltar and south-west Iceland: International Journal of Climatology, v. 17, p. 1433 –1450.

Luterbacher, J., Xoplaki, E., Dietrich, D., Jones, P.D., Davies, T.D., Portis, D., Gonzalez-Rouco, J.F., von Storch, H., Gyalistras, D., Casty, C., and Wanner, H., 2001, Extending North Atlantic Oscillation reconstructions back to 1500: Atmospheric Science Letters, v. 2, p. 114-124.

Mutvei, H., Dunca, E., Timm, H., and Slepukhina, T., 1996, Structure and growth rates of bivalve shells as indicators of environmental changes and pollution: Bulletin de l'Institut océanographique, Monaco, v. 14, 65-72.

Schöne, B.R., 2003, A 'clam-ring' master-chronology constructed from a short-lived bivalve mollusc from the northern Gulf of California, USA: The Holocene, v. 13, p. 39-49.

Schöne, B.R., and Bentley, D., 2002, Use of HMDS (hexamethyldisilazane) to dry organic microstructures in etched bivalve mollusk and barnacle shells: Nautilus, v. 116, p. 25-31.

Torrence, C., and Compo, G., 1998, A Practical Guide to Wavelet Analysis: Bulletin of the American Meteorological Society, v. 79, p.61-78.

Torrence, C., and Webster, P.J., 1999, Interdecadal changes of the ENSO-monsoon system: Journal of Climate, v. 12, p. 2679-2690.

Appendix Figure Captions

Figure DR1. Etched cross-section of an *Arctica islandica* shell. Annual growth breaks are indicated by symbols.

Figure DR2. Individual SGI curves of *Arctica islandica*. Visual comparison reveals a high degree of running similarity.

Figure DR3. Arithmetic mean curves of the NOR and CNS chronologies. The 95% confidence intervals for each SGI value are provided.

Figure DR4. Number of specimens used per year.

Figure DR5. Continuous-wavelet spectra (Morlet wavelet, wave number = 6) of WNAO indices based on instrumental measurements (Hurrell, 1995) and on bivalves (NOR—Norwegian Sea; CNS—central North Sea). Common spectral peaks occur at 7–9 and 5–7 yr and are intermittently stronger and weaker. Amplitudes are scaled with variance of respective index. Edge effects can underestimate amplitudes outside cone of influence (black line). Periods in hatched area should not be interpreted.

Figure DR6. Wavelet cross-scalograms of the following WNAO pairs: (1) *A. islandica*-based WNAO index – Hurrell's (1995) instrumental WNAO, (2) *A. islandica*-based WNAO index – Jones' et al. (1997) instrumental WNAO, (3) *A. islandica*-based WNAO index – Luterbacher's et al. (1997) proxy WNAO, (4) *A. islandica*-based WNAO index – Cook's et al. (2002) proxy WNAO, (5) *A. islandica*-based WNAO index – Glueck and Stockton's (2001) proxy WNAO.

Figure DR7. Running correlation coefficients calculated in a sliding 30-yr window between our new *A. islandica*-based WNAO index and instrumental and other proxy WNAO records.

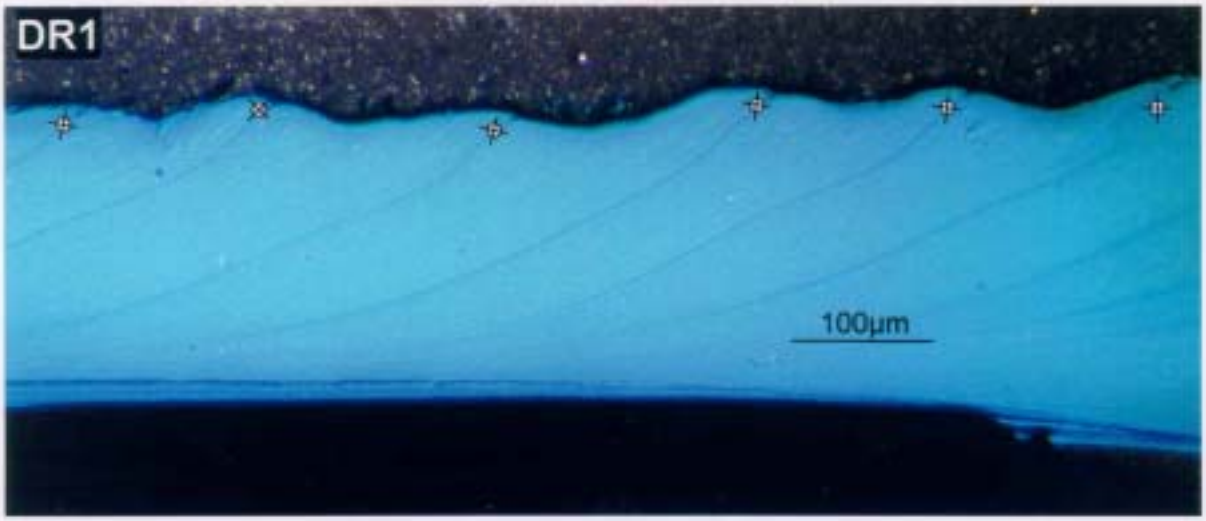
DR1
100µm

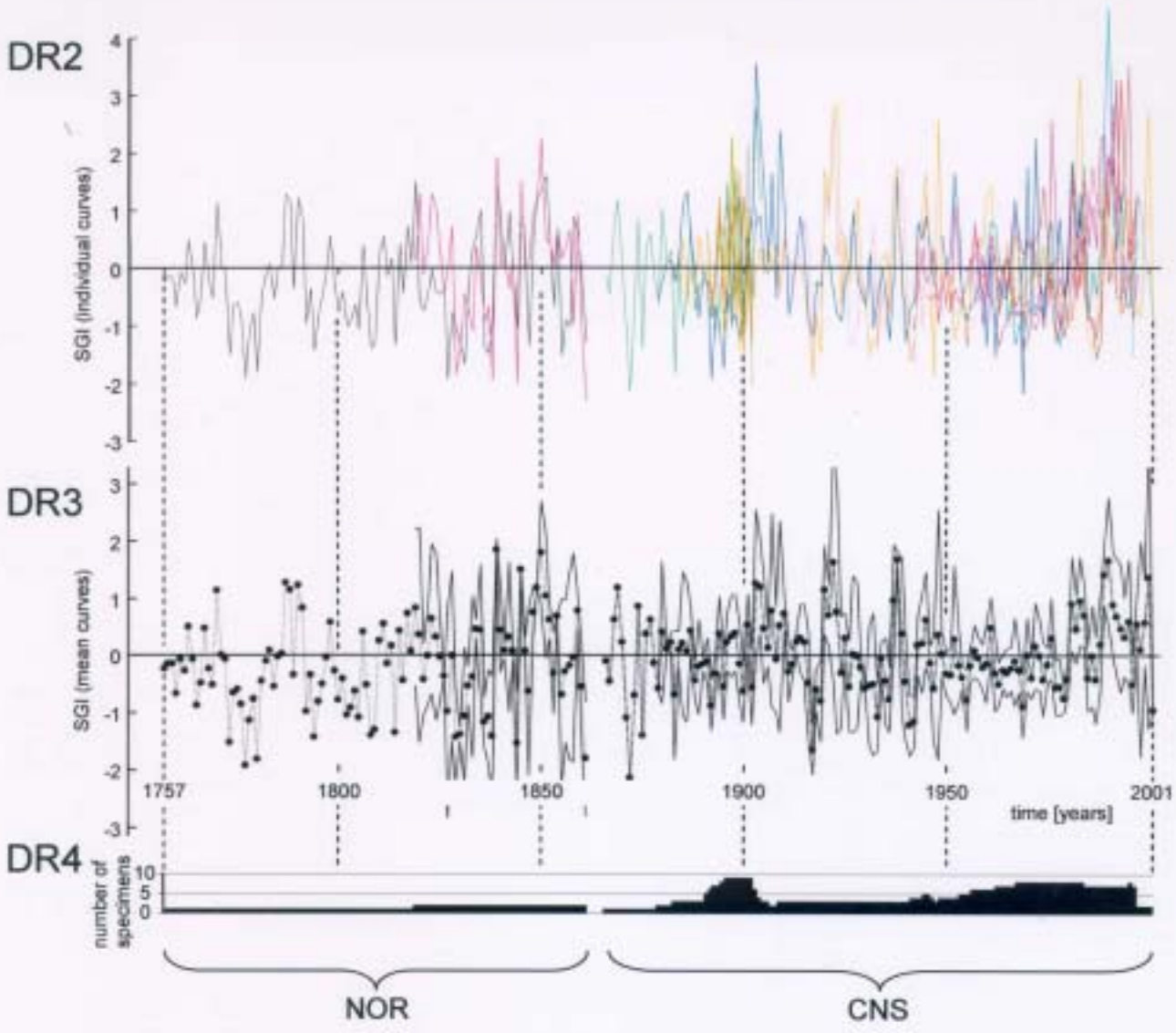
DR2
SGI (individual curves)
DR3
SGI (mean curves)
1757
1800
1850
1900
1950
2001
time [years]
DR4
number of specimens
10
5
0
NOR
CNS

Schöne et al.
Appendix Figs
DR5+6

DR5

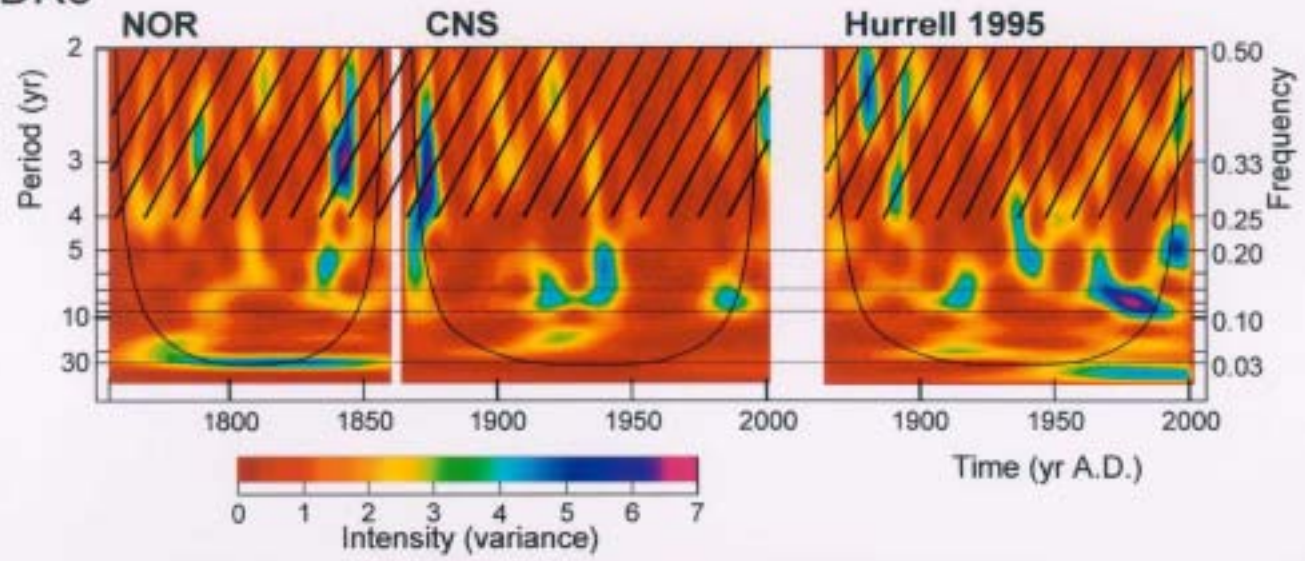

DR6

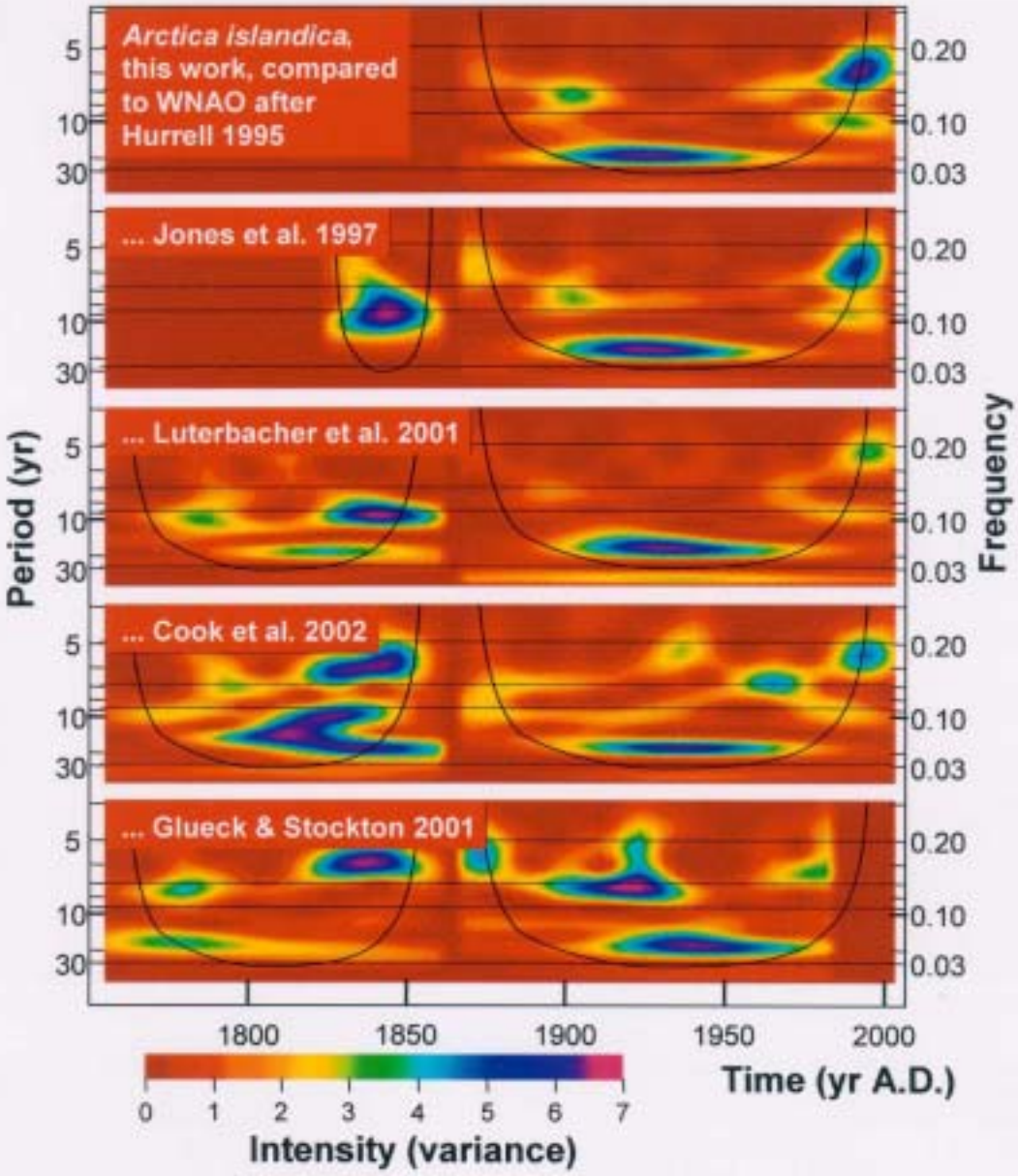

Schöne et al.
Appendix Fig
DR7

DR7